Biosynthetic Method and Characterization of Hydrozincite Nanoparticles Using Rubus Ellipticus Smith

R. Mithra

mithraravi212@gmail.com

Government Arts College

S. Venkateshwari

Government Arts College

Article

Keywords:

Posted Date: April 21st, 2026

DOI: https://doi.org/10.21203/rs.3.rs-9120118/v1

Additional Declarations: No competing interests reported.

7. BIOSYNTHETIC METHOD AND CHARACTERIZATION OF HYDROZINCITE NANOPARTICLES USING RUBUS ELLIPTICUS SMITH

[1]*R. MITHRA -mithraravi212@gmail.com [2*]S. Venkateshwari

Govt. Arts College, Udhagamandalam India

7.1 INTRODUCTION

Nanotechnology relates the area of science and engineering which uses nanoscale dimensions for characterization, structure and development of materials[1]. Now-a-days, nanomaterials have proven their ability to offer a long term practical solutions to an array of world wide issues[2]. On a global scale, research and development in this field continues to develop[3]. When a material approaches closer to nanoscale range the properties get modified[4].

Biological method is the most widely used technique for the synthesis in recent days[5]. Any part of the plant which are used for the synthesis of nanoparticles are known as bio-synthetic or green synthesis method[6]. This technique does not consume high pressure, heat, energy and hazardous chemicals[7]. Parts of the plant are an alluring venue due to the low cost cultivation, safety, rapid production time and capacity to boost the results for the fabrication of nanomaterials[8].

One of the most widely utilized metal oxide nanoparticle is Zinc oxide because they are easy to synthesis and exhibit low level of toxicity[9]. Zinc oxide possess a band gap of 3.37eV and the exciton binding energy of 60meV at room temperature[10][11]. ZnO is a n-type semiconductor with amazing chemical, physical and thermal stabilities[5]. The mineral Hydrozincite often occurs in masses or crusts, sometimes mistaken with others minerals like calcite[12][13].

In the current chapter, Hydrozincite was synthesized using the Rubus Ellipticus Smith fruit. Rubus Ellipticus is a shrub type plant with 1meter -3meter in height. The native of this plant is Sri Lanka, China, Indonesia, Philippines and subcontinent of India[14][15][16]. The fruit is also known as Himalayan Raspberry or Golden raspberry which belongs to Rosaceae family[14][15][17]. In Nilgiris, Tamilnadu, India the fruit bears the tamil/local name as Mullu Pazham(MPM). Indian Himalayan region is very popular for its high bio-diversity, where more than 670 wild species are consumed for health beneficiary supplements[18]. The plant bears leaves with some prickles on it[16]. Image of the plant was shown in Fig 7.1. It bears small flowers which are white in color with five petals in it. The fruits were obovate shaped with golden yellow in color[19]. The unripe fruits were green in color and the ripened

fruits were yellow in color[15]. The fruits has tiny white color seeds which are enclosed by the fleshy part and can be consumed as such. The flowers and fruits usually grow in clusters. The flowering season of this plant was from February to April and the fruiting season was from June to September[19].

Fig7.1: Plant of MPM

The taxonomical classification of the species is given below:

Kingdom : Plantae
Clade : Angiosperms
Order : Rosales
Family : Rosaceae
Genus : Rubus
Species : R. Ellipticus

The Rubus Ellipticus fruit resembles like Raspberry and Blueberry and has similar taste and health benefits[18]. The fruit has a natural colorants due to the presence of anthocyanins which was proved in previous work by Tarun Kumar, et al, 2023[16]. The stem and leaves has the presence of glycosides, flavonoids, terpenes, lipids, vitamins, phenols, ascorbic acids, amino acids etc.[18][15][20]. The plant has wound healing property due to its antitumor, antidiabetic and antioxidant activity[17][21]. Renal tonic and anti – diuretic properties were widely recognized in shoots and roots of this plant[15]. The roots, leaves and stem plays a vital role in Ayurveda, traditional Chinese medicine and in folk therapies[18]. The fruit has the presence of bioactive compounds due to which it is used in cosmetic, food, nutraceutical and in medical field to heal cough, fever, diarrhea, dysentery, vomiting and treating wounds[18][14][15]. The taste of the ripened fruit was sour and sweet[19]. The image of the flower and fruits were given in Fig 7.2 and Fig 7.3 respectively.

Fig 7.2: Flowers and unripe fruits of MPM **Fig 7.3: Ripened fruits of MPM**

7.2: COLLECTION OF FRUITS AND PREPARATION OF FRUIT POWDER

The fruits of Rubus Ellipticus Smith was collected near the college campus, Government Arts College, Ooty, Tamil Nadu, India. The ripened fresh fruits has hairy texture, soft in nature which can be easily pressed by hand. The stalk base was removed from the fruits and the whole fruits were taken and cleaned for the characterization studies. The fruits were washed twice with tap water until the dust particles are removed. These fruits were then washed with distilled water to remove the ions and water soluble impurities. The collected fruits were showed in the Fig 7.4. Then the fruits were shade dried at room temperature. It took 3 weeks to get dry completely. The dried fruits got shrinked in size and was hard as their moisture content was lost. This was shown in Fig 7.5. The dried fruits were ground into powder using mortar and pestle. Powder of MPM was stored in an air tight container for further studies which was shown in Fig 7.6.

Fig 7.4: Fresh fruits of MPM **Fig7.5: Dried fruits** **Fig.7.6 Powder of MPM**

7.2.1 PREPARATION OF MPM AQUEOUS EXTRACT

The aqueous extract of MPM was prepared by reflux method as shown in Fig 7.7. 10g of MPM powder was measured and mixed with 200ml of distilled water. This mixture was refluxed at 90^{o}c for approximately one hour so that the MPM powder gets easily absorbed in the water. After the mixture cools down to room tempertaure the round bottom flask was removed from the heating mantle and the extract was poured to a beaker. The MPM extract was collected and filtered twice using whatmann no.1 filter paper to remove the impurities. The prepared fruit extract was yellow in colour as shown in Fig 7.8.

Fig 7.7: Reflux process

Fig 7.8: Filtered solution of MPM fruit extract

7.2.2 PREPARATION OF HYDROZINCITE NANOPARTICLES USING TPM

100ml of distilled water was added to 2.19g of Zinc Acetate salt to prepare 0.1M of Zinc Acetate solution. The solution was stirred for about 45 minutes for the salt to get dissolved completely. The Zinc acetate solution was clear and the MPM extract was yellow in colour. The MPM extract was added to Zinc acetate solution at 1:1 ratio. The mixture was heated to 100^{o}c and stirred at around 530rpm for about 1 hour. The colour of the solution has changed from yellow to brown. This brown solution was kept covered for a couple of days without disturbing for the particles to get settle down. The prepared solution was tightly covered with a paper to prevent the dust particles to enter the solution or contaminated or oxidised. The sedimented particles was shown in Fig 7.9.

Fig 7.9: Sedimented particles from MPM fruit extract

The sedimented particles were brown in colour and those particles were taken and transferred into another beaker. In order to separate the colloidal solution of the sedimented particles the solution were centrifuged for 45 minutes at 1000rpm. The obtained particles were washed with distilled water to remove the water soluble impurities and centrifuged again for 30 min at 1000rpm. Then the particles were dried in oven for 30 minutes at 100^0C to remove the moisture content in the prepared nano particles. The collected dried particles was shown in Fig 7.10.

Fig7.10: Dried synthesized nanoparticle

7.3 RESULT AND DISCUSSION

7.3.1 XRD ANALYSIS

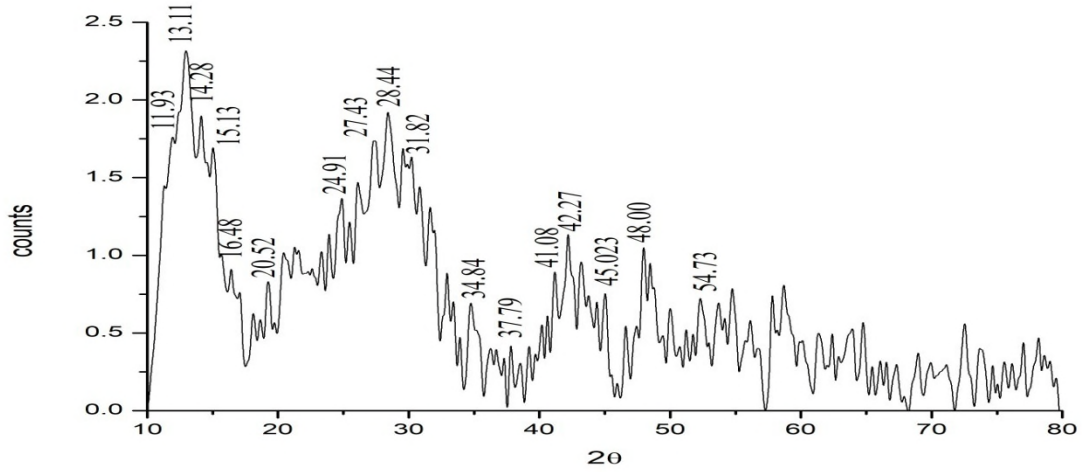

Fig 7.11: XRD spectra of the synthesized sample using MPM fruit extract

X-ray diffraction (XRD) spectra is a widely employed technique which is used to understand the phase identification of different crystalline materials such as nanopowders, solid-state compounds and thin films[22]. Fig 7.11 shows the XRD pattern for the synthesized particle using MPM fruit extract. X-axis represents 2θ value ranging between 10^0 to 80^0 and the Y-axis scale represents the counts from 0.0 to 2.5. The synthesized sample reveals 2θ peaks at 11.93, 13.11, 14.28, 15.13, 16.48, 20.52, 24.91, 27.43, 28.44, 31.82, 34.84, 37.79, 41.08, 42.27, 45.02, 48.00 and 54.73. The assigned hkl values of the obtained peaks are 310, 200, 020, 021, 001, 201, 310, 401, 020, 220, 202, 511, 402, 022, 701, 220 and 113 respectively. The observed peak values coincides with the peak values of JCPDS card no. 00-019-1458 of Hydrozincite with its corresponding peaks as 12.9, 17.0, 18.1, 22.6, 23.1, 28.5, 30.0, 33.2, 36.2, 41.2, 43.1, 47.7[23][24][25]. The obtained 2θ values and the corresponding hkl values predicts that the prepared particle has monoclinic structure[26][27]. Peak at a 2θ value of 13.11 strongly suggests that Hydrozincite consititutes the primary phase within the sample[28][29]. Crystallite size for the synthesized particle was calculated from Debye-Scherrer formula mentioned in equation (1) in chapter 3. The peaks at the 2θ value of 13.11, 16.48, 28.44, 34.84 and 42.27 with minimal disruption to the crystallinity shows the formation of well-defined periodic structure with relatively large crystallite size[30]. Peak broadening shows the irregular distribution in the interlayer spacing between Zinc atoms, suggesting lattice strain and reduced crystallite size[30]. The observed broadening of the peaks noticed at the 2θ values 24.91, 27.43,31.82 is an indicative of nanometer crystallite size of the synthesized sample[31][32][33]. Obtained 2θ values and their corresponding FWHM

values and calculated crystallite size are tabulalted in Table 7.1. From the Fig 7.11 the unassigned peaks observed at the 2θ values 14.28, 15.13, and 20.52, which are not consistent with the standard JCPDS card no. 00-019-1458 were attributed to the impurity phases. The impurity phases might be due to the presence of bio-organic elements from the fruit extract.

Table.7.1: Values of 2θ, FWHM and their calculated crystallite size of the prepared sample

S.No.	2 θ	FWHM	Calculated Crystallite Size
1	11.93	3.76647	2.2149
2	13.11	0.30412	27.47181
3	14.28	0.33996	24.59362
4	15.13	0.73076	11.45329
5	16.48	0.30369	27.60467
6	20.52	0.64389	13.094
7	24.91	2.09553	4.05411
8	27.43	0.64976	13.14264
9	28.44	0.12611	67.92862
10	31.82	3.15747	2.73136
11	34.84	0.19173	45.30334
12	41.08	0.62619	14.15555
13	42.27	0.25569	34.78351
14	48.00	0.23235	39.12984
15	54.73	0.3127	29.83171

The average crystallite size (D) of the synthesized particle was calculated to be 23.83nm. The dislocation density was calculated as 1.761 x $10^{-3}$$nm^{-2}$ from the obtained crystallite size (D).

7.3.2 UV ANALYSIS

UV spectroscopy detects the absorption of ultraviolet light by molecules, enabling precise analysis of electronic structures and concentration levels in diverse chemical systems[34]. The formation of nanoparticles can be studied using this technique[35][36]. Fig 7.12 shows the UV spectra for synthesized particle using MPM extract.

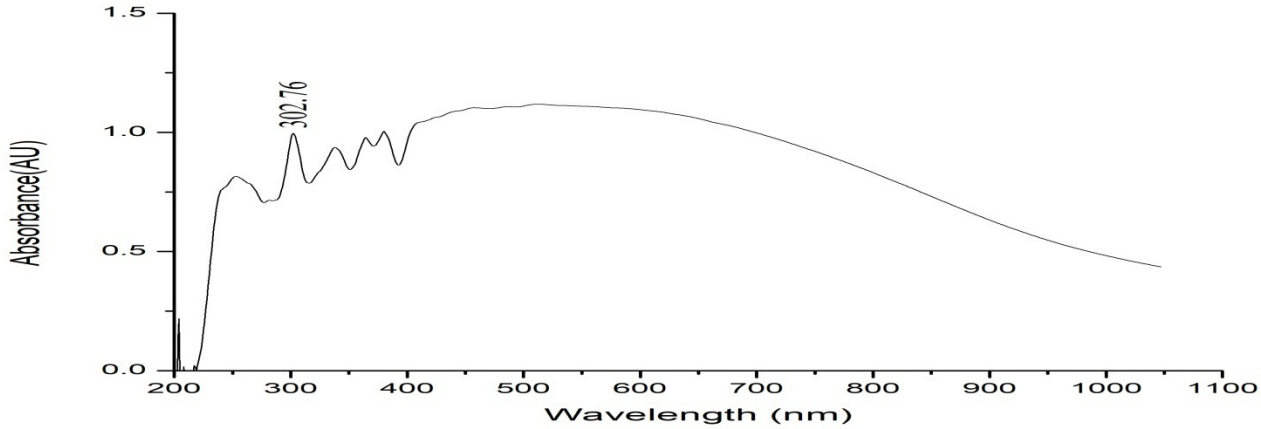

Fig7.12: UV spectra of the synthesized sample using MPM fruit extract

Wavelength in nm was marked in X-axis where the scale ranges between 200nm to 1100nm with a step size of 100nm. Aborbance in AU was marked in Y-axis where the scale ranges between 0.0AU to 1.5AU with a step size of 0.5AU. From Fig 7.12 the maximum absorbance peak was noticed at 302.76nm. The observed absorbance peak lies under blue shift region which confirms that the particle is in the scale of nano range[35]. Blue shift in the UV spectrum arises due to quantum confinement effect[37]. The observed sharp peak at 302.76nm indicates the monodispersed character of the synthesized sample[38][39]. The inherent band-gap absorption at the peak value of 302.76nm shows the transition of lone pair electrons from bonding to anti-bonding state[5]. Multiple minor peaks indicates the structural heterogeneity or surface-bound species[40]. After 500nm the absorption peak gradually decreases. The optical band-gap energy was calculated using band-gap energy formula given in equation (4) in chapter 3. The optical band gap energy for the observed maximum absorption peak was calculated to be 4.10eV. The wide band gap indicates that the synthesized material behaves as an insulator, yet it can exhibit appreciable electrical conductivity under ambient conditions[41].

5.3.3 FT-IR ANALYSIS

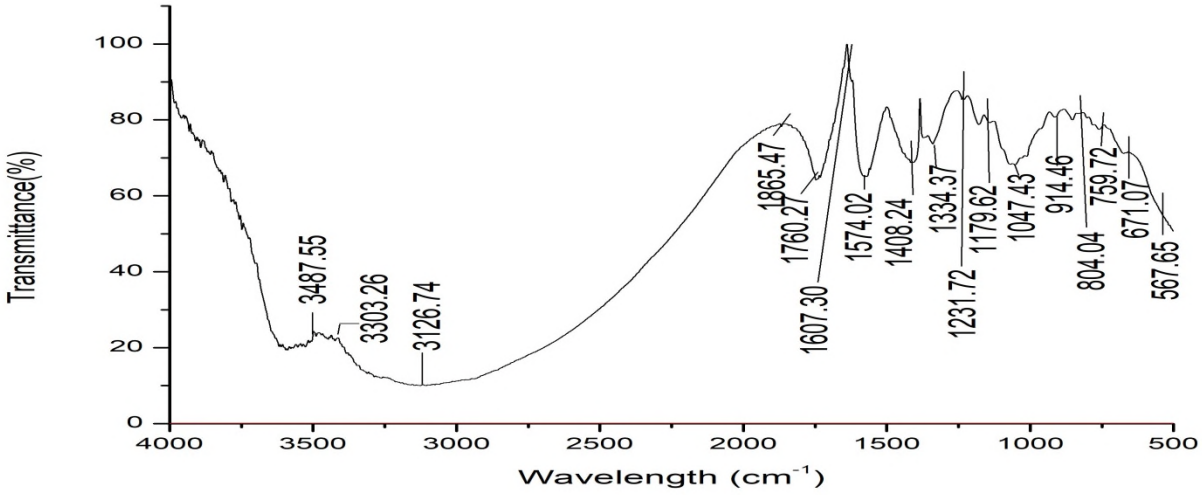

Fig.7.13: FT-IR spectra of the synthesized sample using MPM extract

Fourier Transform Infrared spectroscopy is a technique used to measure the quantity of electromagnetic radiation that is absorbed at the wavelengths beneath 4000^{-1}- $400cm^{-1}$ mid infrared spectrum[42]. Using this technique the molecular species associated with the sample were investigated[43]. Functional groups, organic and inorganic compounds were identified using this technique[44][45]. FT-IR spectra for the prepared sample is displayed in Fig 7.13. The various functional groups involved in the sample was noticed with different peak vibration at the wavelength of $3487.55cm^{-1}$, $3393.26cm^{-1}$, $3126.74cm^{-1}$, $1760.27cm^{-1}$, $1607.30cm^{-1}$, $1574.02cm^{-1}$, $1408.24cm^{-1}$,$1334.37cm^{-1}$, $1231.72cm^{-1}$, $1047.43cm^{-1}$, $914.46cm^{-1}$, $804.04cm^{-1}$, $759.72cm^{-1}$, $671.07cm^{-1}$ and $567.65cm^{-1}$. The peak at $3487.55cm^{-1}$ corresponds to O-H stretching which shows the indication of adsorbed H_2O species[33][46]. Stretching of O-H vibration was observed at the peak $3393.26cm^{-1}$ where the formation of Hydrozincite was confirmed[23][24]. The peak at $3126.74cm^{-1}$ shows C-H stretching vibration with the prescence of Carboxylic acid. Peak arised at $1760.27cm^{-1}$ shows the presence of carboxylic acid and owing to the combination mode in Hydrozincite[24]. Peak observed at $1607.30cm^{-1}$ was due to the strong interaction of C=O with Hydrozincite[30][28]. Peak at $1574.02cm^{-1}$ shows the amorphous state of the synthesized sample and it was allocated to the carboxylate symmetric and asymmetric stretching vibration from the precursor of acetate anion[47][29]. Peak raised at $1408.24cm^{-1}$ shows O-H bending vibration with the presence of Carboxylic acid[29]. Anti symmetric O-H bending were liable for the peak arasied at $1334.37cm^{-1}$ which was due to the free CO_3^{2-} ions[25]. Peak at 1231.72 was due to C-O stretching which shows the presence of alkyl aryl ether (Hydrocarbon) group. The peak raised at $1047.43cm^{-1}$ was

due to C-O stretching which shows the carbonate group[48]. The non-planar vibrational band peaks observed at 914.46cm^{-1}, 804.04cm^{-1} and was due to the unbound CO_3^{2-} ions and also confirming the characteristic features of the synthesized Hydrozincite material[25]. In Fig 7.13 the fingerprint region peaks at 759.72cm^{-1}, 567.65cm^{-1} and 671.07cm^{-1} shows the presence of Zinc oxide which is a mixture of Hydrozincite[33][47][49]. Observed peaks and their corresponding wavelength are tabulated in Table 7.2. Analyzing the peaks in the Fig 7.13(FT-IR spectra) confirmes that the prepared nanoparticles are Hydrozincite.

Table 7.2: FT-IR peaks and their corresponding functional groups

S.No	Wavelength	Assignment	Functional Groups
1	3487.55	O-H stretching	Alchols
2	3393.26	O-H stretching	Alchols, Hydrozincite
3	3126.74	C-H stretching	Carboxylic acid
4	1760.27	C-O stretching	Carboxylic acid
5	1607.30	C=O stretching	Conjugated alkene
6	1574.02	C=C stretching	Cyclic alkene
7	1408.24	O-H bending	Carbonate
8	1334.37	O-H bending	Phenol
9	1231.72	C-O stretching	Alkyl aryl ether
10	1047.43	C-O stretching	Carboxylic acid
11	914.46	C=C bending	Alkene
12	804.04	C=C bending	Alkene
13	759.72	Metal-Oxygen stretching	ZnO[47][49]
14	671.07	Metal-Oxygen stretching	ZnO[47][49]
15	567.65	Metal-Oxygen stretching	ZnO[33][47]

7.3.4 EDX ANALYSIS

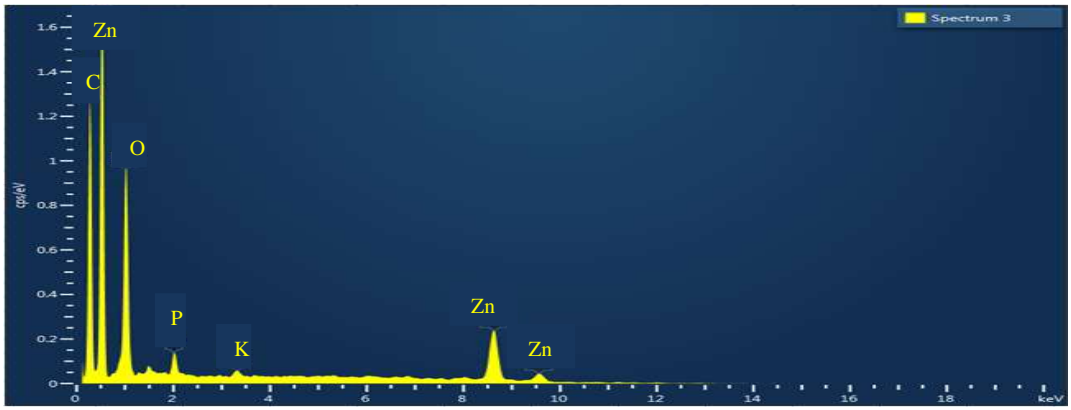

Fig 7.14: EDX spectra of the synthesized sample using MPM fruit extract

The Energy Dispersive X-ray spectroscopy is used to examine the chemical characterization and the elemental composition of the sample by revealing the identifiable peaks[43][50]. The purity of the sample can also be examined using this technique[4]. The composition of elements present in the synthesized sample were shown in the Fig 7.14. Energy is denoted in X-axis whereas counts per electron volt is denoted in Y-axis. According to Fig 7.14 the elements noticed in the spectra are Zinc, Carbon, Oxygen, Phosphour and Potassium. The atomic and molecular weight of each observed elements are tabulated in Table 7.3. The traces of Zinc was observed by three peaks which arises due to the electronic transition from M-shell to L-shell and L-shell to K-shell[51]. Zinc retains its atomic and molecular weight as 58.47% and 45.13% respectively. The atomic and molecular weight percentage of Carbon was noticed as 37.4% and 38.45% respectively. For Oxygen it was noticed as 3.69% and 15.49% respectively. For Phosphour the atomic and molecular weight was noticed as 0.37% and 0.73% respectively. The atomic and molecular weight of Potassium was noticed as 0.08% and 0.2% respectively. The traces of Phosphour and Potassium were in negligible quantity that might be due to presence of the bio-organic compounds raised from the fruit extract[52]. The excitation of Zinc ions has different energy values such as 0.5KeV, 8.5KeV and 9.5KeV. Carbon ions has a energy value of 0.3 KeV, Oxygen ions has a energy value of 1KeV, Phosphour has a energy value of 2KeV and Potassium has a energy value of 3.4KeV respectively. The presence of Phosphour and Potassium confirmed through EDX analysis correlates with the minor impurity phases observed in XRD analysis.

Table 7.3: Atomic and Molecular weight of obtained chemicals from EDX spectra.

S.No	Elements	Atomic Weight	Molecular Weight	Energy Value
1	Zinc	58.47	45.13	9KeV
2	Carbon	37.4	38.45	0.3KeV
3	Oxygen	3.69	15.49	1KeV
4	Phosphor	0.37	0.73	2KeV
5	Potassium	0.08	0.2	3.4KeV

The elements seen in EDX spectra confirms that the prepared nanoparticle is Hydrozincite ($Zn_5(CO_3)_2(OH)_6$) which is the combination of Zinc, Carbon and Oxygen[48][53][54].

7.3.5 SCANNING ELECTRON MICROSCOPY ANALYSIS

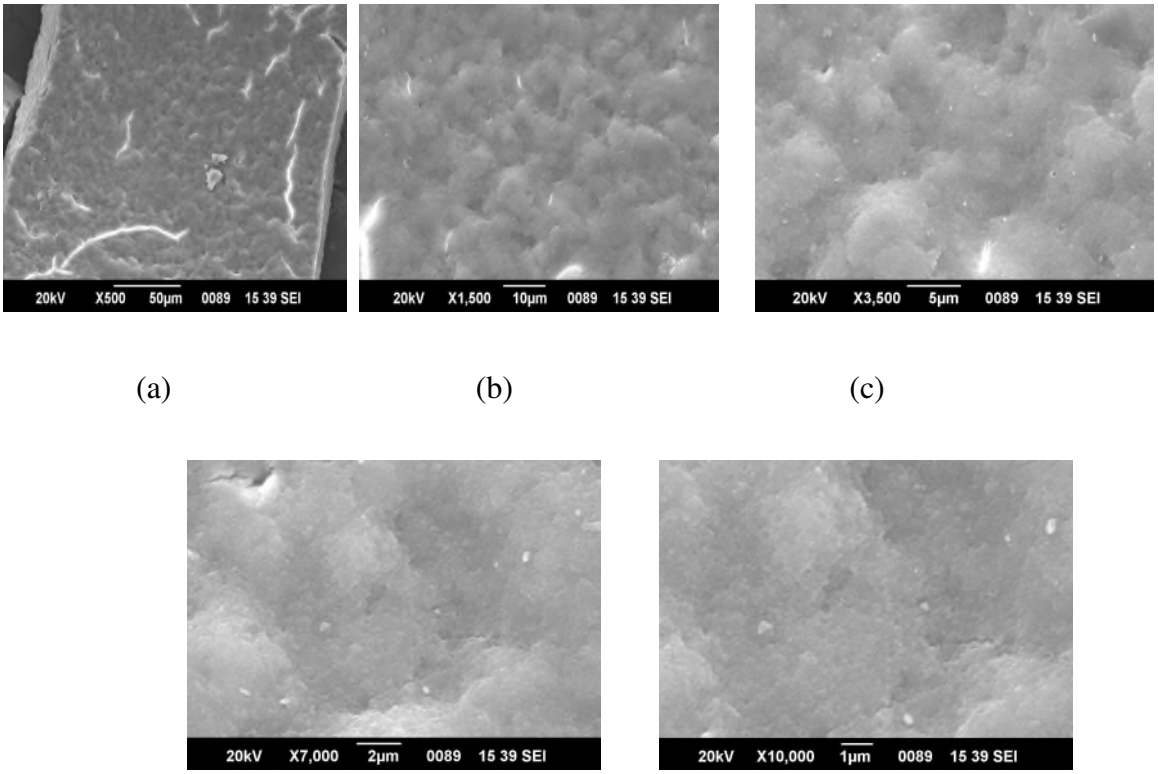

(a) (b) (c)

(d) (e)

Fig.7.15: SEM images of the synthesized sample using MPM fruit extract (a :50µm, b:10µm, c:5µm, d:2µm, e:1µm)

Scanning Electron Microscopy is used to examine the materials which are in nano scale range[42]. The surface morphology of the synthesized sample can be studied through this technique[54]. The morphology of synthesized Hydrozincite particle were shown in Fig 7.15 at different magnifications. At 50µm magnification [Fig 7.15(a)] the acquired image morphology was like a plane sheet surface that resembled a cotton bed like structure[30][55]. Homogeneous distribution of the particles were observed throughout image. Sheet like surface arises due to the layered structures present in Hydrozincite[30]. In Fig 7.15(b) at the magnification of 10µm, the image still shows a flat and spongy surface. The surface maintained its spongy and flat surface at 5µm magnification as shown in Fig 7.15(c). The image seems more spongy in nature when additional magnification is increased to 2µm and 1µm as shown in Fig 7.15(d) and (e). The spongy surface indicates the formation of mesoporous aggregates, suggesting high surface area and interconnected pore structures[27]. Although there are some minimal luminescence which might due to the presence of bio-organic elements like Phosphor and Potassium arised from the fruit extract[56][57]. Presences of Phosphour and Potassium were confirmed through EDX analysis.

5.3.6 TGA-DSC ANALYSIS

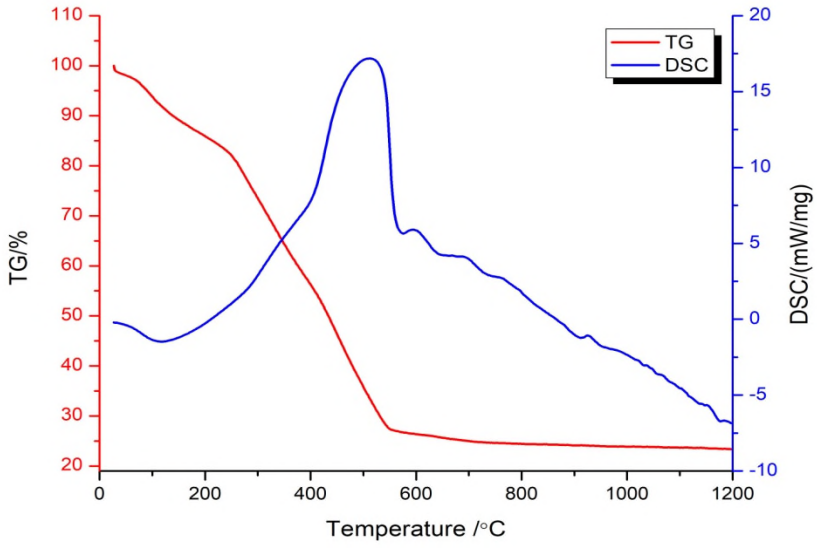

Fig 7.16: TGA-DSC curve of the synthesized sample using MPM fruit extract

Thermo Graviometric Analysis supplies data regarding the mass, weight loss and the content in the stabilizing agents[42][32]. Thermo-oxidative deconstruction of the sample can

be noticed in TGA curve[23]. The TGA-DSC of the synthesized sample using MPM fruit extract was shown in Fig 7.16. The TGA curve gives information on degradation, vaporization of sample with respect to time at different temperture[42]. In Fig 7.16 the Red colour line indicates the TGA curve. For TGA, temperature in ºC was observed in X-axis whereas TG in % was observed in Y-axis. The specimen was heated upto 1200ºC from room temperature with the increase of 200ºC per minute. The initial loss of mass noticed upto 200ºC was due to the release of water content in the sample which was adsorbed on the surface of the molecule[25][28]. Second phase denotes the major mass loss of the specimen from 250ºC upto 530ºC. A single step decomposition process can be observed in Fig 7.16 which attributes to the chage in the crystal structure due to the combination of two phases[58]. Conversion of Hydrozincite into Zinc Oxide with the removal of CO_2 and H_2O was noticed at this second stage[58][28]. After 600ºC it reaches a constant phase. The weight loss was calculated as 13.61% in the first phase, in the second decomposition phase the loss of weight was calculated as 58.22%, and a minor loss at third phase was calculated as 2.86%. Conversion of Zno from Hydrozincite observed during the second stage of decomposition process(as in Fig 7.16) was represented in equation 7.1.

$$Zn_5(CO_3)_2(OH)_6 \longrightarrow 5ZnO + 2CO_2 + 3H_2O \quad (7.1)$$

Differential Scanning Calorimetry (DSC) is a thermo analytical method which measures the variation in the amount of heat required to increase the temperature of the specimen[50]. From Fig 7.16 the obtained spectra shows a sharp exothermic peak at around 400ºC - 600ºC which was denoted by a blue colour line. Sharp peak denotes the removal of water content[13][28]. The exothermic effect of the material is linked to the disintegration of the grafted layers[59]. The peak shows the exothermic effect as the synthesized material undergoes crystallization process[50]. After 600ºC crystallization process decreases slowly. Another small exothermic peaks was noticied at 600ºC and at 900ºC. Thereafter the specimen gradually shifts to the melting phase.

7.3.7. ANTI-MICROBIAL ACTIVITY

7.3.7.1 ANTI-BACTERIAL ACTIVITY

When the bacteria's are treated with antibiotics, their ability to multiply gets restricted typically[60]. The synthesized nano particle and the fruit extract powder were characterized for anti-bacterial activity. In this activity the synthesized nano particle was indicated as NS and the MPM fruit extract was indicated as FE. Fig 7.17 shows the anti-bacterial activity results for the synthesized nanoparticle and the fruit extract. The activity were characterized for gram positive and gram negative bacterial strains. Staphylococcus aureus and Enterococcus faecalis were the gram positive strains. The gram negative bacterial strains used are Escherichia coli and Klebsiella pneumonia. The standard anti-bacterial agent utilized in the activity was Ciprofloxacin. The activity was performed using disc-diffusion method and the culture was grown overnight by using cotton swabs. The diameter of the rings formed around the sample is measured by Zone of inhibition (ZOI). It allows to study the effectiveness of the sample against the bacterial strains. Table 7.4 lists the measured ZOI for every bacterial stains. The percentage of inhibition was calculated with reference to Ciprofloxacin as mentioned in equation (5) in chapter 3. As shown in Fig 7.17 (a) NS showed 13mm ZOI with 35% of efficacy and FE showed 7mm ZOI for with 18% efficacy for Staphylococcus aureus. As shown in Fig 7.17 (b) NS showed 13mm ZOI with 52% of efficacy for and FE showed 15mm ZOI with 60% of efficacy for Enterococcus faecalis. For the gram negative bacterial strains as shown in Fig 7.17 (c) NS showed 10mm ZOI with 34% of efficacy and FE showed 15mm ZOI with 51% of efficacy for Escherichia coli. As shown in Fig 7.17 (d) NS showed 10mm ZOI with 35% of efficacy and FE showed 15mm ZOI with 53% of efficacy for Klebsiella pneumonia. NS exhibited an improved and stronger anti-bacterial activity than FE for all the tested bacterial strains.

Table 7.4 : Results of Anti-bacterial activity along with their efficacy

S.NO	Microorganisms	NS	FE	Ciprofloxacin	Efficacy with reference to Ciprofloxacin	
		Zone of inhibition in mm			NS	FE
1.	*Staphylococcus aureus*	13	07	37	35%	18%
2.	*Enterococcus faecalis*	15	13	25	60%	52%
3.	*Escherichia coli*	15	10	29	51%	34%
4.	*Klebsiella pneumoniae*	15	10	28	53%	35%

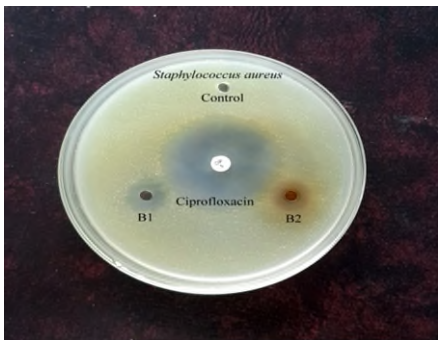

(a)

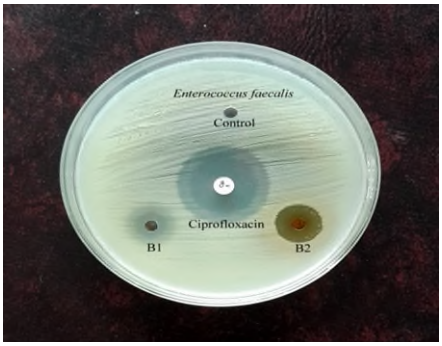

(b)

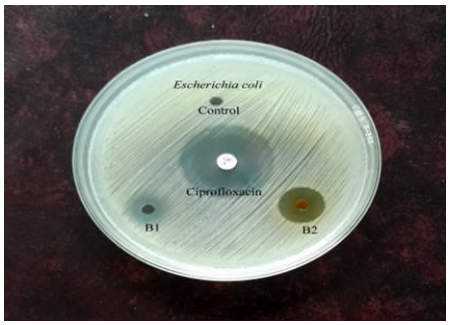

(c)

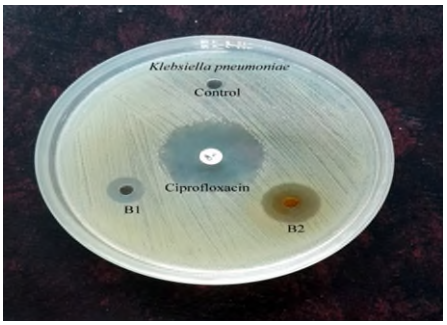

(d)

Fig 7.17: Anti-bacterial activity for the synthesized nanoparticle and MPM fruit extract

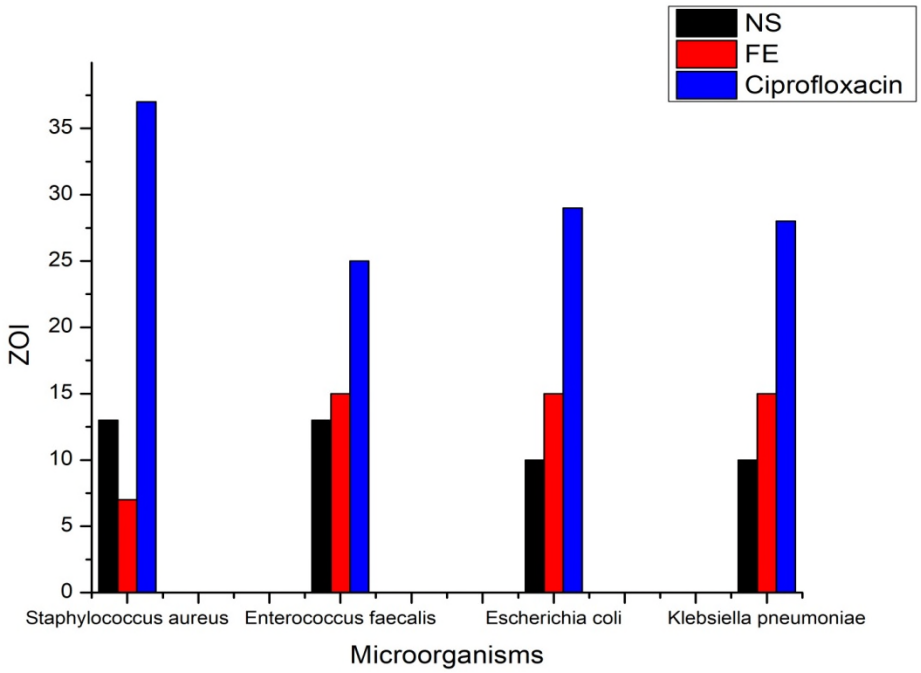

Fig 7.18: Comparative anti-bacterial activity

The antibacterial efficacy of both the synthesized sample and the fruit extract against multiple bacterial strains is compared in Fig 7.18, which exhibits the differences in inhibition efficiency. All the tested bacterial strains are arranged in increasing order based on their performance against NS and FE.

Enterococcus faecalis > Klebsiella pneumonia > Escherichia coli > Staphylococcus aureus

The presence of Phosphour and Potassium in fruit extract which was confirmed through EDX analysis plays a significant role in anti-bacterial activity. Phosphour helps in the synthesis of bioactive substances by improving the metabolic pathways. Whereas Potassium maintains cellular ion balance and improves the cell structures, making bacteria more vulnerable. When combined, these components strengthen and stabilize the antibacterial substances, thereby inhibiting the growth of bacteria[61][62].

In addition to increase the effectiveness of bioactive chemicals in plant extracts, Zinc demonstrates antibacterial activity by rupturing bacterial membranes, producing reactive oxygen species, and blocking vital enzymes[63][64].

Thus the enhanced antibacterial activity of NS compared to FE can be attributed to the combined presence of Zinc, Phosphorus and Potassium, which act synergistically to inhibit the bacterial growth.

7.3.7.2 ANTI-FUNGAL ACTIVITY

Anti-fungal activity was carried using the same process as in anti-bacterial activity. The anti-fungal activity was determined by treating fungal cultures at defined concentrations and incubating them under suitable conditions. The killing of the fungi may occur by destruction of the cell wall, leading to osmotic lysis. The fungal strains employed for the activity are Aspergillus niger, Aspergillus fumigatus, Penicillum sps and Candida albicans. Ketoconazole was taken as standard anti-fungal agent in this activity. Antifungal activity for the synthesized nanoparticle (NS) and the fruit extract (FE) was depicted in Fig 7.19, and ZOI values for each fungus with reference to Ketoconazole were tabulated in Table 7.5. The percentage of inhibition was calculated with reference to Ketoconazole as mentioned in equation (5) in chapter 3. The presence of Zinc in NS exerts a direct effect by disrupting fungal cell membranes and interfering with enzymatic processes[65]. Phosphorus promotes the synthesis of secondary metabolites with antifungal properties, while Potassium strengthens cell walls and maintains osmotic balance, making fungal penetration more difficult. Together these elements act synergistically, stabilizing and potentiating the bioactive compounds in the fruit extract, resulting in effective inhibition of fungal growth[61][62]. As in Fig 7.19(a) NS showed 10mm ZOI with 76% of effectiveness and FE showed 8mm ZOI with 61% of effectiveness for Aspergillus niger. As in Fig 7.19(b) NS showed 8mm ZOI with 80% of effectiveness and FE showed 5mm ZOI with 50% of effectiveness for Aspergillus fumigatus. As in Fig 7.19(c) NS showed 9mm ZOI with 90% of effectiveness and FE showed 4mm ZOI with 40% of effectiveness for Pencillium sps. As in Fig 7.19(d) NS showed 10mm ZOI with 66% of effectiveness and FE showed 7mm ZOI with 46% of effectiveness for Candida albicans. Among all the tested fungal strains, Aspergillus niger showed good response against NS and FE with reference to Ketoconazole. The tested fungal strains are arranged in an increasing order based on their performance against NS and FE.

Aspergillus niger > Candida albicans > Pencillium sps > Aspergillus fumigatus

Table 7.5: Results of Anti-fungal activity along with their efficacy

S.NO	Microorganisms	NS	FE	Ketoconazole	Efficacy with reference to Ketoconazole	
		Zone of inhibiton in mm			NS	FE
1.	*Aspergillus niger*	10	08	13	76%	61%
2.	*Aspergillus fumigatus*	08	05	10	80%	50%
3.	*Penicillum sps*	09	04	10	90%	40%
4.	*Candida albicans*	10	07	15	66%	46%

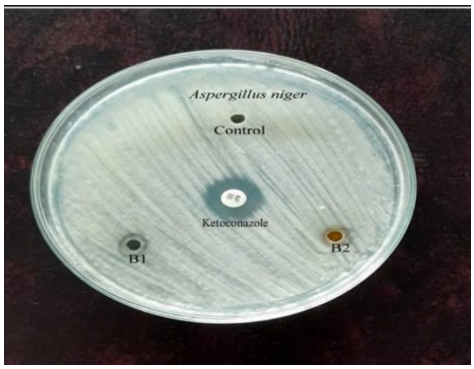

(a)

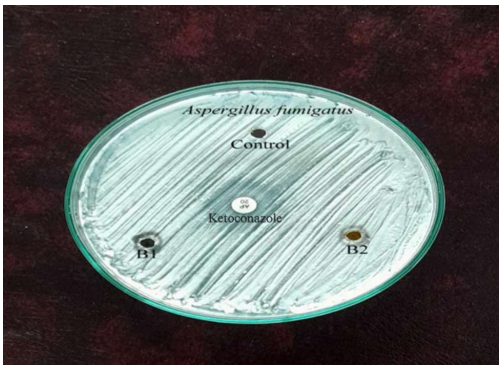

(b)

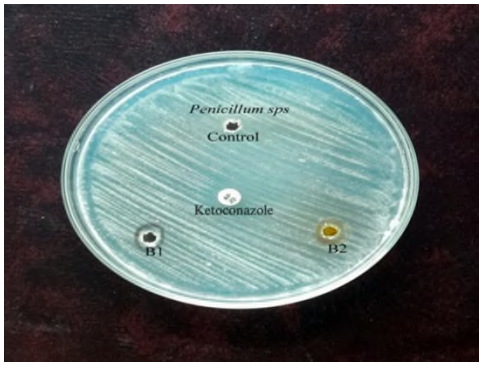

(c)

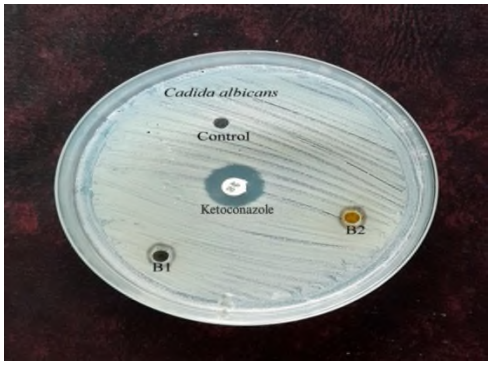

(d)

Fig 7.19: Anti-fungal activity for synthesized nanoparticle and MPM fruit extract

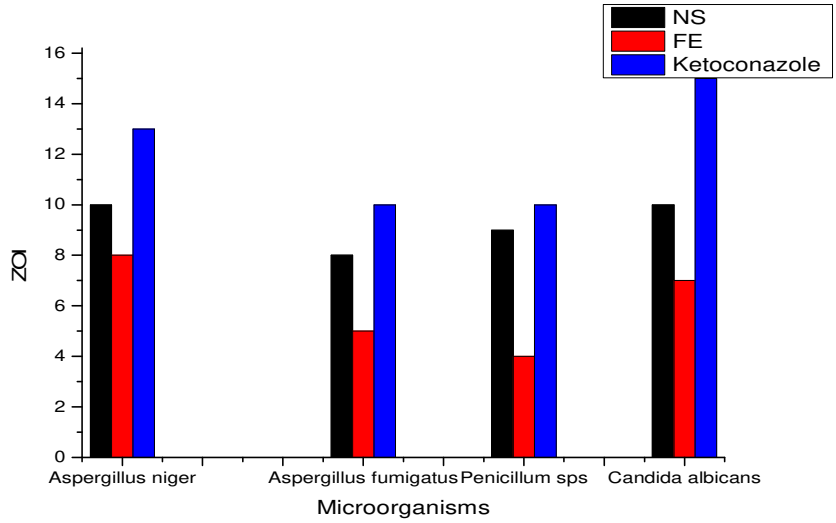

Fig 7.20: Comparative anti-fungal activity

Fig 7.20 illustrates a bar graph comparing the antifungal activity of the synthesized sample and the fruit extract against different fungal strains. Thus from the overall result good anti-fungal activity was observed for the synthesized nanoparticles than the fruit extract. The antifungal activity of the synthesized nanoparticle (NS) is enhanced due to the presence of Zinc, Phosphorus and Potassium.

No funding was obtained for this project work.

DATA AVAILABILITY

All the data characterization studies were done in STIC(SAIF) Cochin sophisticated Lab, Cochin, Kerala, India. The datasets used and/or analysed during the current study available from the corresponding author on reasonable request.

References:

[1] N. Jayarambabu, K. V. Rao, and Y. T. Prabhu, "BENEFICIAL ROLE OF ZINC OXIDE NANOPARTICLES ON GREEN CROP BENEFICIAL ROLE OF ZINC OXIDE NANOPARTICLES ON GREEN CROP PRODUCTION Introduction : Nanotechnology is the term given to those areas of science and," *Int. J. Multidiscip. Adv. Res. trends*, vol. 10, no. February, pp. 273–282, 2015.

[2] A. Alhadhrami, G. G. Mohamed, A. H. Sadek, S. H. Ismail, and A. A. Ebnalwaled, "Behavior of Silica Nanoparticles Synthesized from Rice Husk Ash by the Sol – Gel Method as a Photocatalytic and Antibacterial Agent," 2022.

[3] C. Vidya, S. Hiremath, M. N. Chandraprabha, M. A. L. Antonyraj, and I. Venu, "Green synthesis of ZnO nanoparticles by Calotropis Gigantea," no. Ncwse, pp. 2012–2014, 2013.

[4] D. Manyasree, K. M. Peddi, and R. Ravikumar, "CuO nanoparticles: Synthesis,

characterization and their bactericidal efficacy," *Int. J. Appl. Pharm.*, vol. 9, no. 6, pp. 71–74, 2017, doi: 10.22159/ijap.2017v9i6.71757.
[5] M. Aminuzzaman, L. P. Ying, W. Goh, and A. Watanabe, "Green synthesis of zinc oxide nanoparticles using aqueous extract of Garcinia mangostana fruit pericarp and their photocatalytic," *Bull. Mater. Sci.*, 2018, doi: 10.1007/s12034-018-1568-4.
[6] E. J. Al-kalifawi, T. M. Al-saadi, S. A. Al-dulaimi, and E. E. Al-obodi, "Biosynthesis of silver nanoparticles by using onion (Allium cepa) extract and study antibacterial activity," no. June 2018, 2015.
[7] A. Bouafia, S. E. Laouini, and M. R. Ouahrani, "REVIEW ARTICLE A Review on Green Synthesis of CuO Nanoparticles using Plant Extract and Evaluation of Antimicrobial Activity," vol. 13, no. February, pp. 65–70, 2020, doi: 10.5958/0974-4150.2020.00014.0.
[8] 4 V. V. Makarov1, 2, A. J. Love3, O. V. Sinitsyna2, 6, S. S. Makarova2, 5, I. V. Yaminsky2 and 2* M. E. Taliansky2, 3, N. O. Kalinina1, "'Green' Nanotechnologies: Synthesis of Metal Nanoparticles Using Plants," no. October 2011, 2016, doi: 10.1039/C1GC15386B.
[9] J. Dhatwalia *et al.*, "Rubus ellipticus Sm. Fruit Extract Mediated Zinc Oxide Nanoparticles: A Green Approach for Dye Degradation and Biomedical Applications(Materials (2022), 15, (3470), 10.3390/ma15103470)," *Materials (Basel).*, vol. 15, no. 23, pp. 1–23, 2022, doi: 10.3390/ma15238308.
[10] A. Sinhamahapatra, A. K. Giri, P. Pal, C. Salt, and S. Pahari, "A rapid and green synthetic approach for hierarchically assembled porous ZnO nanoflakes with enhanced catalytic activity," no. June 2014, 2012, doi: 10.1039/C2JM32998K.
[11] S. R. Brintha and M. Ajitha, "Synthesis and characterization of ZnO nanoparticles via aqueous solution , sol-gel and hydrothermal methods," vol. 8, no. 11, pp. 66–72, 2015, doi: 10.9790/5736-081116672.
[12] M. C. Hales and R. L. Frost, "Synthesis and vibrational spectroscopic characterisation of synthetic hydrozincite and smithsonite," *Polyhedron*, vol. 26, no. 17, pp. 4955–4962, 2007, doi: 10.1016/j.poly.2007.07.002.
[13] M. C. H. and R. L. Frost• and Inorganic, "Thermal analysis of smithsonite and hydrozincite Matthew," pp. 0–17, 2008.
[14] R. K. Joshi, L. F. Laurindo, P. Rawat, R. D. A. Goulart, and S. M. Barbalho, "Himalayan Yellow Raspberry (Rubus ellipticus Smith .): A Plant with Multiple Medicinal Purposes," vol. 2, no. December, pp. 59–74, 2022.
[15] P. Aspects, "Yellow Himalayan Raspberry (Rubus ellipticus Sm .):," pp. 1–17, 2023.
[16] I. Tandem and M. Spectrometry, "Separation Of Anthocyanins From Himalayan Yellow Raspberry Rubus Ellipticus Using High-Resolution Liquid Chromatography − Electrospray SEPARATION OF ANTHOCYANINS FROM HIMALAYAN YELLOW RASPBERRY RUBUS ELLIPTICUS USING HIGH- RESOLUTION LIQUID CH ROMATOGRAPH," no. December, 2023, doi: 10.48047/ecb/2023.12.si10.00499.
[17] L. N. Khanal *et al.*, "Green Synthesis of Silver Nanoparticles from Root Extracts of Rubus ellipticus Sm . and Comparison of Antioxidant and Antibacterial Activity," vol. 2022, 2022.
[18] P. Kewlani, D. Tiwari, S. Rawat, and I. D. Bhatt, "Pharmacological and phytochemical potential of Rubus ellipticus: a wild edible with multiple health benefits," *J. Pharm. Pharmacol.*, vol. 75, no. 2, pp. 143–161, 2023, doi: 10.1093/jpp/rgac053.
[19] P. Nagar, "DIVERSITY AND CHARACTERIZATION OF EDIBLE FUTURE FRUITS OF UTTARA KANNADA AND NILGIRIS OF THE WESTERN GHATS IN SOUTH INDIA," vol. LXIII, no. 1, 2019.

[20] A. Khan, N. Ahmad, H. Fazal, M. Ali, and F. Akbar, “RSC Advances Biogenic synthesis of silver nanoparticles using Rubus fruticosus extract and their antibacterial e ffi cacy against Erwinia caratovora and Ralstonia solanacearum phytopathogens,” pp. 5754–5763, 2024, doi: 10.1039/d3ra06723h.
[21] S. Khalil *et al.*, “Antibacterial , antioxidant and photocatalytic activity of novel Rubus ellipticus leaf mediated silver nanoparticles,” *J. Saudi Chem. Soc.*, vol. 27, no. 1, p. 101576, 2023, doi: 10.1016/j.jscs.2022.101576.
[22] C. F. Holder and R. E. Schaak, “Tutorial on Powder X-ray Diffraction for Characterizing Nanoscale Materials,” *ACS Nano*, vol. 13, no. 7, pp. 7359–7365, 2019, doi: 10.1021/acsnano.9b05157.
[23] V. Sharma, S. Basak, K. Rishabh, H. Umaria, and S. W. Ali, “Synthesis of zinc carbonate nanoneedles , a potential flame retardant for cotton textiles,” *Cellulose*, vol. 5, 2018, doi: 10.1007/s10570-018-1962-5.
[24] N. Kanari, D. Mishra, I. Gaballah, and B. Dupré, “Thermal decomposition of zinc carbonate hydroxide,” vol. 410, pp. 93–100, 2004, doi: 10.1016/S0040-6031(03)00396-4.
[25] M. T. Dieng, B. D. Ngom, P. D. Tall, and M. Maaza, “Biosynthesis of Zn 5 (CO 3) 2 (OH) 6 from Arachis Hypogaea Shell (Peanut Shell) and Its Conversion to ZnO Nanoparticles,” vol. 7, no. 1, pp. 1–9, 2019, doi: 10.12691/ajn-7-1-1.
[26] L. Yun, G. Peng, and T. Xi, “Green synthesis of ZnO 2 nanoparticles from hydrozincite and hydrogen peroxide at room temperature,” *Mater. Lett.*, vol. 64, no. 14, pp. 1647–1649, 2010, doi: 10.1016/j.matlet.2010.04.022.
[27] G. De Giudici *et al.*, “Structural properties of biologically controlled hydrozincite: An HRTEM and NMR spectroscopic study,” *Am. Mineral.*, vol. 94, no. 11–12, pp. 1698–1706, 2009, doi: 10.2138/am.2009.3181.
[28] M. Y. Nassar, M. M. Moustafa, and M. M. Taha, “Hydrothermal tuning of the morphology and particle size of hydrozincite nanoparticles using different counterions to produce nanosized ZnO as an efficient adsorbent for textile dye removal†,” *RSC Adv.*, vol. 6, no. April, pp. 42180–42195, 2016, doi: 10.1039/C6RA04855B.
[29] T. Biswick, W. Jones, A. Pacuła, E. Serwicka, and J. Podobinski, “Evidence for the formation of anhydrous zinc acetate and acetic anhydride during the thermal degradation of zinc hydroxy acetate, Zn5(OH)8(CH3CO2)2·4H2O to ZnO,” *Solid State Sci.*, vol. 11, no. 2, pp. 330–335, 2009, doi: 10.1016/j.solidstatesciences.2008.06.018.
[30] K. Suzuki, H. Miyamura, and J. Balachandran, “One-pot hydrothermal synthesis of carbon dots-immobilized hydrozincite for ZnO-based nanocomposite lighting applications,” *J. Asian Ceram. Soc.*, vol. 9, no. 4, pp. 1473–1480, 2021, doi: 10.1080/21870764.2021.1995939.
[31] A. C. Mohan and B. Renjanadevi, “Preparation of Zinc Oxide Nanoparticles and its Characterization Using Scanning Electron Microscopy (SEM) and X-Ray Diffraction(XRD),” *Procedia Technol.*, vol. 24, pp. 761–766, 2016, doi: 10.1016/j.protcy.2016.05.078.
[32] S. Zhang, H. Fortier, and J. R. Dahn, “Characterization of zinc carbonate hydroxides synthesized by precipitation from zinc acetate and potassium carbonate solutions,” vol. 39, pp. 1939–1948, 2004, doi: 10.1016/j.materresbull.2004.05.023.
[33] R. Wahab, S. G. Ansari, Y. S. Kim, M. A. Dar, and H. Shin, “Synthesis and characterization of hydrozincite and its conversion into zinc oxide nanoparticles,” vol. 461, pp. 66–71, 2008, doi: 10.1016/j.jallcom.2007.07.029.
[34] T. Surya, “Core Principles and Varied Applications of Ultraviolet (UV) Spectroscopy in Analytical Chemistry,” pp. 1–2, doi: 10.35248/2471-2698.23.8.221.Citation.

[35] P. Wilson and S. Venkateshwari, “Green Synthesis of Silver Nano Particles using Ageratina Adenophora Leaf Extract,” no. December, 2020.
[36] D. O. F. Philosophy and I. N. Physics, “GREEN SYNTHESIS CHARACTERIZATION AND ANTIMICROBIAL ACTIVITY OF SILVER NANOPARTICLES FROM THE NILGIRIS,” 2022.
[37] M. P. Y. S. P. K S Pavithra1, Fasiulla1 and 1Department, “Effect of microwave irradiation power for the morphological changes of ZnO nanoparticles Effect of microwave irradiation power for the morphological changes of ZnO nanoparticles,” 2019, doi: 10.1088/1757-899X/577/1/012120.
[38] S. Talam, S. R. Karumuri, and N. Gunnam, “Synthesis , Characterization , and Spectroscopic Properties of ZnO Nanoparticles,” vol. 2012, 2012, doi: 10.5402/2012/372505.
[39] M. S. Alwhibi, D. A. Soliman, A. Alonaizan, N. Abdulhaq, M. El-zaidy, and M. S. Alsubeie, “Journal of King Saud University – Science Green biosynthesis of silver nanoparticle using Commiphora myrrh extract and evaluation of their antimicrobial activity and colon cancer cells viability,” *J. King Saud Univ. - Sci.*, vol. 32, no. 8, pp. 3372–3379, 2020, doi: 10.1016/j.jksus.2020.09.024.
[40] L. A. and D. Nedeltcheva, “Resolution of overlapping UV–Vis absorption bands and quantitative analysis,” pp. 217–227, 2000, doi: 10.1039/a900007k.
[41] K. C. Kao, “Electrical conduction and breakdown in insulating polymers,” *Proc. IEEE Int. Conf. Prop. Appl. Dielectr. Mater.*, vol. 1, pp. 1–17, 2000, doi: 10.1109/icpadm.2000.875620.
[42] S. Mourdikoudis and R. M. Pallares, “Characterization techniques for nanoparticles : comparison and complementarity upon studying,” pp. 12871–12934, 2018, doi: 10.1039/c8nr02278j.
[43] K. M. Mbae and S. Umesha, “Green synthesis of silver nanoparticles by Rivina humilis leaf extract to tackle growth of Brucella species and other perilous pathogens,” 2020.
[44] A. M. Awwad and N. M. Salem, “Green Synthesis of Silver Nanoparticles byMulberry LeavesExtract,” *Nanosci. Nanotechnol.*, vol. 2, no. 4, pp. 125–128, 2012, doi: 10.5923/j.nn.20120204.06.
[45] A. I. Journal, A. Chahardoli, N. Karimi, F. Sadeghi, and A. Fattahi, “Green approach for synthesis of gold nanoparticles from Nigella arvensis leaf extract and evaluation of their antibacterial , antioxidant , cytotoxicity and catalytic activities,” *Artif. Cells, Nanomedicine, Biotechnol.*, vol. 0, no. 0, pp. 579–588, 2018, doi: 10.1080/21691401.2017.1332634.
[46] F. Wypych, G. G. Carbajal Arízaga, and J. E. F. Da Costa Gardolinski, “Intercalation and functionalization of zinc hydroxide nitrate with mono- and dicarboxylic acids,” *J. Colloid Interface Sci.*, vol. 283, no. 1, pp. 130–138, 2005, doi: 10.1016/j.jcis.2004.08.125.
[47] M. Bitenc, M. Marinšek, and Z. Crnjak Orel, “Preparation and characterization of zinc hydroxide carbonate and porous zinc oxide particles,” *J. Eur. Ceram. Soc.*, vol. 28, no. 15, pp. 2915–2921, 2008, doi: 10.1016/j.jeurceramsoc.2008.05.003.
[48] Z. Li, X. Shen, X. Feng, P. Wang, and Z. Wu, “Non-isothermal kinetics studies on the thermal decomposition of zinc hydroxide carbonate,” vol. 438, pp. 102–106, 2005, doi: 10.1016/j.tca.2005.08.026.
[49] T. L. Valerio, G. A. R. Maia, L. F. Gonçalves, A. Viomar, E. P. Banczek, and P. R. P. Rodrigues, “Study of the Nb 2 O 5 Insertion in ZnO to Dye-sensitized Solar Cells 2 . Material and Methods,” *Mater. Res.*, vol. 22, pp. 1–5, 2019.
[50] A. Alasadi and J. K. Behera, “SYNTHESIS AND CHARACTERIZATION OF ZnO

NANO-PARTICLES Submitted," no. December, p. 184, 2018, [Online]. Available: http://etheses.whiterose.ac.uk/22820/

[51] Jeffrey B. Kortright and Albert C. Thompson, "X-Ray Data Booklet Table 1-2. Photon energies, in electron volts, of principal K-, L-, and M-shell emission lines," *Lawrence Berkeley Natl. Lab.*, 1979.

[52] P. W. S.Venkateshwari**s, "CHARACTERIZATION AND GREEN SYENTHESIS OF SILVER NANO PARTICLES FROM SALVIA OFFICINALIS LEAF EXTRACT," vol. 8, no. 7, pp. 1–23, 2022.

[53] S. Ghose, " The crystal structure of hydrozincite, Zn 5 (OH) 6 (CO 3) 2 ," *Acta Crystallogr.*, vol. 17, no. 8, pp. 1051–1057, 1964, doi: 10.1107/s0365110x64002651.

[54] T. Alhawi, M. Rehan, D. York, and X. Lai, "Synthesis of Zinc Carbonate Hydroxide Nanoparticles Using Microemulsion Process," *Procedia Eng.*, vol. 102, pp. 346–355, 2015, doi: 10.1016/j.proeng.2015.01.158.

[55] A. Obata, K. Mori, K. Inukai, K. Kato, G. Poologasundarampillai, and T. Kasuga, "Three-Dimensional Cotton-Wool-Like Polyhydroxybutyrate/Siloxane-Doped Vaterite Composite Fibrous Scaffolds: Effect of Imogolite-Coating on Physicochemical and Cell Adhesion Properties," *Front. Mater.*, vol. 7, no. February, pp. 1–11, 2020, doi: 10.3389/fmats.2020.00033.

[56] S. Pinnioja, M. Siitari-kauppi, J. Jernstro, and A. Lindberg, "Detection of irradiated foods by luminescence of contaminating mineralsÐe ect of mineral composition on luminescence intensity," vol. 55, pp. 743–747, 1999.

[57] R. Kumar *et al.*, "Site-selective mapping of metastable states using electron-beam induced luminescence microscopy," *Sci. Rep.*, vol. 10, no. 1, pp. 1–30, 2020, doi: 10.1038/s41598-020-72334-7.

[58] T. Alhawi, M. Rehan, D. York, and X. Lai, "Hydrothermal Synthesis of Zinc Carbonate Hydroxide Nanoparticles," *Procedia Eng.*, vol. 102, pp. 356–361, 2015, doi: 10.1016/j.proeng.2015.01.161.

[59] M. Grochowicz, B. Gawdzik, M. Jaćkowska, and B. Buszewski, "Thermal characterization of polymeric anion exchangers with a dendrimeric structure," *J. Therm. Anal. Calorim.*, vol. 114, no. 3, pp. 955–961, 2013, doi: 10.1007/s10973-013-3096-1.

[60] H. S. Bhargav, S. D. Shastri, S. P. Poornav, K. M. Darshan, and M. M. Nayak, "Measurement of the Zone of Inhibition of an Antibiotic," *Proc. - 6th Int. Adv. Comput. Conf. IACC 2016*, pp. 409–414, 2016, doi: 10.1109/IACC.2016.82.

[61] E. A. Do and C. M. Gries, "Beyond homeostasis: Potassium and pathogenesis during bacterial infections," *Infect. Immun.*, vol. 89, no. 7, pp. 1–16, 2021, doi: 10.1128/IAI.00766-20.

[62] L. Zhang *et al.*, "Black Phosphorus – A Rising Star in the Antibacterial Materials," *Int. J. Nanomedicine*, vol. 18, no. November, pp. 6563–6584, 2023, doi: 10.2147/IJN.S438448.

[63] R. Krishnamoorthy *et al.*, "Antibacterial Mechanisms of Zinc Oxide Nanoparticle against Bacterial Food Pathogens Resistant to Beta-Lactam Antibiotics," *Molecules*, vol. 27, no. 8, pp. 1–17, 2022, doi: 10.3390/molecules27082489.

[64] A. Sirelkhatim *et al.*, "Review on zinc oxide nanoparticles: Antibacterial activity and toxicity mechanism," *Nano-Micro Lett.*, vol. 7, no. 3, pp. 219–242, 2015, doi: 10.1007/s40820-015-0040-x.

[65] H. S. Elshafie, A. Osman, M. M. El-saber, I. Camele, and E. Abbas, "Antifungal Activity of Green and Chemically Synthesized ZnO Nanoparticles against Alternaria citri , the Causal Agent Citrus Black Rot," vol. 39, no. 3, pp. 265–274, 2023.